American Mineralogist, Volume 99, pages 218–224, 2014

Vanadio-oxy-dravite, $NaV_3(Al_4Mg_2)(Si_6O_{18})(BO_3)_3(OH)_3O$, a new mineral species of the tourmaline supergroup

Ferdinando Bosi[1,*], Henrik Skogby[2], Leonid Reznitskii[3] and Ulf Hålenius[2]

[1]Dipartimento di Scienze della Terra, Sapienza Università di Roma, P.le A. Moro, 5, I-00185 Rome, Italy
[2]Department of Geosciences, Swedish Museum of Natural History, Box 50007, SE-10405 Stockholm, Sweden
[3]Institute of the Earth's Crust, Siberian Branch, Russian Academy of Science, Lermontova str., 128, 664033 Irkutsk, Russia

Abstract

Vanadio-oxy-dravite, $NaV_3(Al_4Mg_2)(Si_6O_{18})(BO_3)_3(OH)_3O$, is a new mineral of the tourmaline supergroup. It is found in metaquartzites of the Pereval marble quarry (Sludyanka, Lake Baikal, Russia) in association with quartz, Cr-V-bearing tremolite and mica, diopside–kosmochlor–natalyite, Cr-bearing goldmanite, escolaite–karelianite, dravite–oxy-vanadium-dravite, V-bearing titanite and rutile, ilmenite, oxyvanite–berdesinskiite, shreyerite, plagioclase, scapolite, zircon, pyrite, and an unnamed oxide of V, Cr, Ti, U, and Nb. Crystals are green, transparent with a vitreous luster, pale green streak, and conchoidal fracture. Vanadio-oxy-dravite has a Mohs hardness of approximately 7½, and a calculated density of 3.14 g/cm^3. In plane-polarized light, vanadio-oxy-dravite is pleochroic (O = yellow green and E = pale olive green) and uniaxial negative: $\omega = 1.693(5)$, $\varepsilon = 1.673(5)$. Vanadio-oxy-dravite is rhombohedral, space group $R3m$, with the unit-cell parameters $a = 16.0273(3)$, $c = 7.2833(1)$ Å, $V = 1620.24(5)$ Å^3, $Z = 3$. Crystal-chemical analysis resulted in the empirical structural formula:

$$^{X}(Na_{0.70}Ca_{0.23}\square_{0.05}K_{0.02})_{\Sigma 1.00}\ ^{Y}(V^{3+}_{1.39}Mg_{1.16}Al_{0.35}Fe^{3+}_{0.04}Ti^{4+}_{0.04}Fe^{2+}_{0.02})_{\Sigma 3.00}$$
$$^{Z}(Al_{3.74}Mg_{1.28}V^{3+}_{0.78}Cr^{3+}_{0.20})_{\Sigma 6.00}\ ^{T}(Si_{6.00}O_{18})\ ^{B}(BO_3)_3\ ^{V}(OH)_3\ ^{W}[O_{0.74}(OH)_{0.26}]_{\Sigma 1.00}.$$

The crystal structure of vanadio-oxy-dravite was refined to an $R1$ index of 1.70% using 1800 unique reflections collected with Mo$K\alpha$ X-radiation. Ideally, vanadio-oxy-dravite is related to oxy-dravite and oxy-vanadium-dravite by the homovalent substitution $V^{3+} \leftrightarrow Al^{3+}$. Tourmaline with chemical compositions classified as vanadio-oxy-dravite can be either Al dominant or V dominant as a result of the compositional boundaries along the solid solution between Al and V^{3+} that are determined at $^{Y+Z}(V_{1.5}Al_{5.5})$, corresponding to $Na^{Y}(V_{1.5}Al_{1.5})^{Z}(Al_4Mg_2)Si_6O_{18}(BO_3)_3(OH)_3O$, and $^{Y+Z}(V_5Al_2)$, corresponding to $Na^{Y}(V_3)^{Z}(V_2Al_2Mg_2)Si_6O_{18}(BO_3)_3(OH)_3O$.

Keywords: Vanadio-oxy-dravite, tourmaline, new mineral species, crystal-structure refinement, electron microprobe, infrared spectroscopy, optical absorption spectroscopy

Introduction

The tourmaline supergroup minerals are widespread, occurring in sedimentary, igneous, and metamorphic rocks (Dutrow and Henry 2011). They are important indicator minerals that can provide information on the compositional evolution of their host rocks, chiefly due to their ability to incorporate a large number of elements (e.g., Novák et al. 2004, 2011; Agrosì et al. 2006; Lussier et al. 2011a; van Hinsberg et al. 2011; Bačík et al. 2012). However, the chemical composition of tourmalines is also controlled by short-range and long-range constraints (e.g., Hawthorne 1996, 2002a; Bosi and Lucchesi 2007; Bosi 2010, 2011, 2013; Henry and Dutrow 2011; Skogby et al. 2012) as well as by temperature (van Hinsberg and Schumacher 2011). Tourmaline supergroup minerals are complex borosilicates and their crystal structure and crystal chemistry have been extensively studied (e.g., Foit 1989; Hawthorne and Henry 1999; Bosi and Lucchesi 2007; Lussier et al. 2008, 2011b; Bosi 2008; Bosi et al. 2010; Filip et al. 2012). In accordance with Henry et al. (2011), the general formula of tourmaline may be written as: $XY_3Z_6T_6O_{18}(BO_3)_3V_3W$, where X ($\equiv {}^{[9]}X$) = Na^+, K^+, Ca^{2+}, $\square$ (= vacancy); Y ($\equiv {}^{[6]}Y$) = Al^{3+}, Fe^{3+}, Cr^{3+}, V^{3+}, Mg^{2+}, Fe^{2+}, Mn^{2+}, Li^+; Z ($\equiv {}^{[6]}Z$) = Al^{3+}, Fe^{3+}, Cr^{3+}, V^{3+}, Mg^{2+}, Fe^{2+}; T ($\equiv {}^{[4]}T$) = Si^{4+}, Al^{3+}, B^{3+}; B ($\equiv {}^{[3]}B$) = B^{3+}; W ($\equiv {}^{[3]}O1$) = OH^{1-}, F^{1-}, O^{2-}; V ($\equiv {}^{[3]}O3$) = OH^{1-}, O^{2-} and where, for example, T represents a group of cations (Si^{4+}, Al^{3+}, B^{3+}) accommodated at the [4]-coordinated T sites. The dominance of these ions at one or more sites of the structure gives rise to a range of distinct mineral species.

Recently, several new minerals of the tourmaline supergroup were approved by the Commission on New Minerals, Nomenclature and Classification (CNMNC) of the International Mineralogical Association (IMA). Among these are several oxy-tourmalines related by complete solid solution in the Al^{3+}-Cr^{3+}-V^{3+} subsystem: oxy-dravite, end-member formula $NaAl_3(Al_4Mg_2)(Si_6O_{18})(BO_3)_3(OH)_3O$ (IMA 2012-004a; Bosi and Skogby 2013), oxy-chromium-dravite, $NaCr_3(Cr_4Mg_2)(Si_6O_{18})(BO_3)_3(OH)_3O$ (IMA 2011-097; Bosi et al. 2012a); oxy-vanadium-dravite, $NaV_3(V_4Mg_2)(Si_6O_{18})(BO_3)_3(OH)_3O$ (IMA

* E-mail: ferdinando.bosi@uniroma1.it

11-E; Bosi et al. 2013a).

A new species of oxy-tourmaline, vanadio-oxy-dravite, has been approved by the IMA-CNMNC (proposal no. 2012-074). The holotype specimen (sample PR73) is deposited in the collections of the Museum of Mineralogy, Earth Sciences Department, Sapienza University of Rome, Italy, catalog number 33068. A formal description of the new species vanadio-oxy-dravite is presented here, including a full characterization of its physical, chemical, and structural properties.

Occurrence, appearance, and physical and optical properties

The crystals of vanadio-oxy-dravite are green and occur in metaquartzites in the Pereval marble quarry, Sludyanka crystalline complex, Southern Baikal region, Russia (51°37′N 103°38′E). The Pereval quarry is the type locality (see Bosi et al. 2012a for a more detailed description) for natalyite, florensovite, kalininite, magnesiocoulsonite, oxy-vanadium-dravite, oxy-chromium-dravite, vanadio-oxy-chromium-dravite, chromo-aluminopovondraite, batisivite, oxyvanite, and cuprokalininite. Minerals associated with the holotype specimen are: quartz, Cr-V-bearing tremolite and muscovite–celadonite, diopside–kosmochlor–natalyite, Cr-bearing goldmanite, escolaite–karelianite, dravite, V-bearing titanite and rutile, ilmenite, oxyvanite–berdesinskiite, shreyerite, plagioclase, scapolite, zircon, pyrite, and an unnamed oxide of V, Cr, Ti, U, and Nb, The host rocks (quartz-diopside) are Cr-V-bearing carbonate-siliceous sediments, metamorphosed to granulite facies and partly diaphtorized (Salnikova et al. 1998) to amphibolite facies (retrograde stage). Vanadio-oxy-dravite was formed in the prograde stage (granulite facies). The crystals are euhedral, reaching up to 0.3 mm in length, and may be chemically zoned (for details, see Fig. 3 of Bosi et al. 2013a), but homogeneous crystals also occur.

The morphology of vanadio-oxy-dravite consists of elongated $\{10\bar{1}0\}$ and $\{11\bar{2}0\}$ prisms terminated by a prominent $\{0001\}$ pedion and small, minor $\{10\bar{1}1\}$ pyramidal faces. Crystals are green, with pale green streak, transparent, and display vitreous luster. They are brittle and show conchoidal fracture. The Mohs hardness is approximately 7½ (Reznitsky et al. 2001). The calculated density is 3.14 g/cm^3. In transmitted light, vanadio-oxy-dravite is pleochroic with O = yellow green and E = pale olive green. Vanadio-oxy-dravite is uniaxial negative with refractive indices, measured by the immersion method using white light from a tungsten source, of $\omega = 1.693(5)$, $\varepsilon = 1.673(5)$. The mean index of refraction, density, and chemical composition lead to excellent compatibility indices ($1 - K_p/K_c = 0.026$) (Mandarino 1976, 1981).

Method

Single-crystal structural refinement

A representative fragment of the type specimen was selected for X-ray diffraction measurements on a Bruker KAPPA APEX-II single-crystal diffractometer, at Sapienza University of Rome (Earth Sciences Department), equipped with a CCD area detector (6.2 × 6.2 cm^2 active detection area, 512 × 512 pixels) and a graphite crystal monochromator, using Mo$K\alpha$ radiation from a fine-focus sealed X-ray tube. The sample-to-detector distance was 4 cm. A total of ca. 3265 exposures (step = 0.2°, time/step = 20 s) covering a full reciprocal sphere with a redundancy of about 8 was used. Final unit-cell parameters were refined by means of the Bruker AXS SAINT program using reflections with $I > 10\sigma(I)$ in the range $5° < 2\theta < 73°$. The intensity data were processed and corrected for Lorentz, polarization, and background effects with the APEX2 software program of Bruker AXS. The data were corrected for absorption using the multi-scan method (SADABS). The absorption correction led to a significant improvement in R_{int}. No violations of $R3m$ symmetry were noted.

Structural refinement was done with the SHELXL-97 program (Sheldrick 2008). Starting coordinates were taken from Bosi et al. (2004). Variable parameters were: scale factor, extinction coefficient, atomic coordinates, site scattering values, and atomic-displacement factors. To obtain the best values of statistical indexes ($R1$, $wR2$), neutral scattering curves were used for all atoms. In detail, the occupancy of the X site was modeled by using the sodium scattering factor, the Y site vanadium and magnesium scattering factors, and the Z site using vanadium and aluminum factors. The T and B sites were modeled, respectively, with Si and B scattering factors and with a fixed occupancy of 1, because refinement with unconstrained occupancies showed no significant deviations from this value. Three full-matrix refinement cycles with isotropic-displacement parameters for all atoms were followed by anisotropic cycles until convergence was attained. No significant correlations over a value of 0.7 between the parameters were observed at the end of refinement. Table 1 lists crystal data, data-collection information, and refinement details; Table 2 gives the fractional atomic coordinates and site occupancies; Table 3 gives the displacement parameters; and Table 4 gives selected bond distances. A further refinement with chemical constraints was done for CIF (on deposit[1]) by modelling the cation occupancy as follows: the X site, by Na vs. Ca; the Y site, by V vs. Mg and with the occupancy of Mg and Cr fixed to the value obtained from the structural formula. The results are statistically equal to those reported in Tables 1–4.

X-ray powder diffraction

Powder X-ray data were was derived from the single-crystal structural refinement since the available sample material was not sufficient for X-ray powder diffraction measurements. Data are listed in Table 5.

Electron-microprobe analysis

Electron-microprobe analyses of the crystal used for X-ray diffraction refinement were obtained by wavelength-dispersive spectrometer (WDS mode) with a

[1] Deposit item AM-14-108, CIF. Deposit items are stored on the MSA web site and available via the *American Mineralogist* Table of Contents. Find the article in the table of contents at GSW (ammin.geoscienceworld.org) or MSA (www.minsocam.org), and then click on the deposit link.

Table 1. Single-crystal X-ray diffraction data: details for vanadio-oxy-dravite

Sample	PR73
Crystal size (mm)	0.10 × 0.16 × 0.24
a (Å)	16.0273(3)
c (Å)	7.2833(1)
V (Å^3)	1620.24(5)
Range for data collection, 2θ (°)	5–73
Reciprocal space range hkl	$-21 \le h \le 25$
	$-23 \le k \le 26$
	$-12 \le l \le 11$
Total number of frames	3265
Set of measured reflections	7988
Unique reflections, R_{int} (%)	1800, 2.10
Redundancy	8
Absorption correction method	SADABS
Refinement method	Full-matrix last-squares on F^2
Structural refinement program	SHELXL-97
Extinction coefficient	0.00007(1)
Flack parameter	0.06(2)
$wR2$ (%)	3.81
$R1$ (%) all data	1.70
$R1$ (%) for $I > 2\sigma(I)$	1.65
GooF	1.060
Largest diff. peak and hole (±e$^-$/Å^3)	0.40 and –0.30

Notes: R_{int} = merging residual value; $R1$ = discrepancy index, calculated from F-data; $wR2$ = weighted discrepancy index, calculated from F^2-data; GooF = goodness of fit; Diff. peaks = maximum and minimum residual electron density. Radiation, Mo$K\alpha$ = 0.71073 Å. Data collection temperature = 293 K. Space group $R3m$; $Z = 3$.

Cameca SX50 instrument at the "Istituto di Geologia Ambientale e Geoingegneria (Rome, Italy), CNR," operating at an accelerating potential of 15 kV and a sample current of 15 nA, with a 10 μm beam diameter. Minerals and synthetic compounds were used as standards: wollastonite (Si, Ca), magnetite (Fe), rutile (Ti), corundum (Al), vanadinite (V) fluorphlogopite (F), periclase (Mg), jadeite (Na), K-feldspar (K), sphalerite (Zn), metallic Cr, Mn, and Cu. The overlap corrections and the PAP routine were applied (Pouchou and Pichoir 1991). The results (Table 6) represent mean values of 10 spot analyses. In accord with the very low concentration of Li in dravitic samples (e.g., Henry et al. 2011), the Li_2O content was assumed to be insignificant. Mn, Zn, Cu, and F were below their respective detection limits (0.03 wt%) in the studied sample.

Infrared spectroscopy

A homogeneous vanadio-oxy-dravite crystal was measured by Fourier transform infrared (FTIR) absorption spectroscopy to characterize (OH) absorption bands in the wavenumber range 2000–5000 cm^{-1} using a Bruker Equinox 55 spectrometer equipped with a NIR source, a CaF_2 beam-splitter, a wire-grid polarizer, and an InSb detector. Polarized spectra with a resolution of 4 cm^{-1} were acquired parallel and perpendicular to the crystallographic **c**-axis direction using a circular measurement area of 100 μm diameter on a 36 μm thick doubly polished crystal plate that had been oriented parallel to the **c**-axis by morphology and optical microscopy. As often observed, fundamental (OH) absorption bands polarized parallel to the **c**-axis direction of tourmalines are exceptionally intense, and it was not possible to thin the sample sufficiently to avoid off-scale absorption intensity for the strongest band (Fig. 1).

Optical absorption spectroscopy

Polarized, room-temperature optical-absorption spectra were recorded on the same 36 μm thick crystal platelet used for the FTIR measurements. The spectra were measured in the range 270–1100 nm (37 037–9091 cm^{-1}) at a resolution of 1 nm using an AVASPEC-ULS2048X16 spectrometer attached via a 400 μm UV optical fiber to a Zeiss Axiotron UV-microscope. A 75 W Xenon arc lamp served as illuminating source and Zeiss Ultrafluar 10× lenses served as objective and condenser. A UV-quality Glan-Thompson prism with a working range from 250 to 2700 nm (40 000 to 3704 cm^{-1}) was used as polarizer. The size of the circular measure aperture was 64 μm in diameter. The wavelength scale of the spectrometer was calibrated against Ho_2O_3 doped and Pr_2O_3/Nd_2O_3 doped standards (Hellma glass filters 666F1 and 666F7) with an accuracy better than 15 cm^{-1} in the wavelength range 300–1100 nm. Recorded spectra were fitted using the Jandel PeakFit 4.12 software assuming Gaussian peak shapes.

TABLE 2. Fractional atom coordinates and site occupancy for vanadio-oxy-dravite

Site	x	y	z	Site occupancy
X	0	0	0.22772(15)	$Na_{1.137(6)}$
Y	0.12347(2)	0.061737(12)	0.63625(6)	$V_{0.513(4)}Mg_{0.487(4)}$
Z	0.29820(2)	0.26190(2)	0.61148(6)	$Al_{0.852(3)}V_{0.148(3)}$
B	0.11004(6)	0.22007(12)	0.4539(2)	$B_{1.00}$
T	0.191020(18)	0.189344(19)	0.000	$Si_{1.00}$
O1 (≡W)	0	0	0.7691(3)	$O_{1.00}$
O2	0.06078(4)	0.12157(8)	0.48340(16)	$O_{1.00}$
O3 (≡V)	0.26119(9)	0.13059(4)	0.51120(17)	$O_{1.00}$
O4	0.09258(4)	0.18516(8)	0.07085(16)	$O_{1.00}$
O5	0.18236(8)	0.09118(4)	0.09011(16)	$O_{1.00}$
O6	0.19403(5)	0.18472(5)	0.77971(12)	$O_{1.00}$
O7	0.28367(5)	0.28332(5)	0.07786(11)	$O_{1.00}$
O8	0.20860(5)	0.26946(6)	0.44063(12)	$O_{1.00}$
H3	0.2565(16)	0.1283(8)	0.393(3)	$H_{1.00}$

TABLE 4. Selected bond distances (Å) for vanadio-oxy-dravite

B-O2	1.384(2)	*Y*-O1	1.9682(10)
B-O8^{A} (×2)	1.3715(11)	*Y*-O2^{B} (×2)	2.0327(8)
<*B*-O>	1.376	*Y*-O3	2.1174(12)
		Y-O6^{C} (×2)	2.0066(8)
T-O4	1.6292(5)	<*Y*-O>	2.027
T-O5	1.6453(5)		
T-O7	1.5995(7)	*Z*-O3	2.0164(6)
*T**-O6	1.6080(9)	*Z*-O6	1.9374(8)
<*T*-O>	1.620	*Z*-O8^{E}	1.9178(8)
		Z-O7^{E}	1.9349(8)
X-O2^{B,F} (×3)	2.5129(13)	*Z*-O7^{D}	1.9836(8)
X-O4^{B,F} (×3)	2.8126(13)	*Z*-O8	1.9492(8)
X-O5^{B,F} (×3)	2.7223(12)	<*Z*-O>	1.957
<*X*-O>	2.683	O3-H	0.86(2)

Notes: Standard uncertainty in parentheses. Superscript letters: A = (*y* – *x*, *y*, *z*); B = (*y* – *x*, – *x*, *z*); C = (*x*, *x* – *y*, *z*); D = (*y* – *x* + 1/3, –*x* + 2/3, *z* + 2/3); E = (–*y* + 2/3, *x* – *y* + 1/3, *z* + 1/3); F = (–*y*, *x* – *y*, *z*). Transformations relate coordinates to those of Table 2.
* Positioned in adjacent unit cell.

TABLE 5. Simulated X-ray powder diffraction data for vanadio-oxy-dravite (λ = 1.5418 Å)

I_{calc} > 9 (%)	d_{calc} (Å)	*h k l*
37	6.4467	1 0 1
19	5.0153	0 2 1
19	4.6185	3 0 0
52	4.2606	2 1 1
66	4.0041	2 2 0
47	3.5221	0 1 2
10	3.0317	4 1 0
67	2.9928	1 2 2
100	2.5958	0 5 1
15	2.3970	2 3 2
15	2.3594	5 1 1
13	2.2091	5 0 2
12	2.1500	0 3 3
11	2.0763	2 2 3
43	2.0573	1 5 2
28	1.9340	3 4 2
20	1.6756	0 6 3
13	1.6520	2 7 1
17	1.6025	5 5 0
15	1.5226	0 5 4
15	1.4704	5 1 4
10	1.4232	4 3 4

Note: *I* = calculated intensity, *d* = calculated interplanar spacing, *hkl* = reflection indices.

TABLE 3. Displacement parameters (Å^2) for vanadio-oxy-dravite

Site	U^{11}	U^{22}	U^{33}	U^{23}	U^{13}	U^{12}	U_{eq}/U_{iso}*
X	0.0149(4)	0.0149(4)	0.0158(5)	0.000	0	0.00743(18)	0.0152(3)
Y	0.00704(16)	0.00604(13)	0.00951(17)	–0.00095(5)	–0.00189(10)	0.00352(8)	0.00742(10)
Z	0.00619(13)	0.00663(13)	0.00729(12)	0.00037(9)	–0.00002(9)	0.00314(10)	0.00673(8)
B	0.0075(4)	0.0083(6)	0.0088(6)	0.0008(5)	0.0004(2)	0.0041(3)	0.0081(3)
T	0.00521(12)	0.00494(11)	0.00708(12)	–0.00055(9)	–0.00045(9)	0.00252(9)	0.00575(6)
O1	0.0104(5)	0.0104(5)	0.0077(8)	0.000	0	0.0052(2)	0.0095(3)
O2	0.0088(3)	0.0052(4)	0.0120(5)	0.0014(3)	0.00071(17)	0.0026(2)	0.0091(2)
O3	0.0179(5)	0.0139(4)	0.0061(5)	0.00053(19)	0.0011(4)	0.0089(3)	0.0122(2)
O4	0.0084(3)	0.0162(5)	0.0094(5)	–0.0009(4)	–0.00045(19)	0.0081(3)	0.0104(2)
O5	0.0158(5)	0.0078(3)	0.0097(5)	0.00071(19)	0.0014(4)	0.0079(3)	0.01019(19)
O6	0.0102(3)	0.0085(3)	0.0068(3)	–0.0014(2)	–0.0008(2)	0.0053(3)	0.00825(13)
O7	0.0079(3)	0.0069(3)	0.0101(3)	–0.0008(2)	–0.0028(3)	0.0014(3)	0.00929(14)
O8	0.0045(3)	0.0097(3)	0.0178(4)	0.0025(3)	0.0009(3)	0.0029(3)	0.01094(15)
H3							0.018*

* Equivalent (U_{eq}) and isotropic (U_{iso}) displacement parameters; H-atom was constrained to have a U_{iso} 1.5 times the U_{eq} value of the O3 oxygen.

Results and discussion

Generval comment

The present crystal-structure refinement and electron-microprobe analyses were obtained from the same single crystal. However, complementary optical and spectroscopic data were recorded from coexisting crystals. Small differences in composition are likely to occur between these crystals.

Determination of atomic proportions

In agreement with the structural-refinement results, the boron content was assumed to be stoichiometric in the vanadio-oxy-dravite sample (B^{3+} = 3.00 apfu). Both the site-scattering results and the bond lengths of *B* and *T* are consistent with the *B* site fully occupied by boron and no amount of B^{3+} at the *T* site (e.g., Hawthorne 1996; Bosi and Lucchesi 2007). In line with the optical absorption results, which show the occurrence of both Fe^{2+} and Fe^{3+} (see below), the Fe contents were calculated on the basis of $Fe^{3+}/\Sigma Fe = 0.68$, measured by Mössbauer spectroscopy (Bosi et al. 2013b) for a Fe-bearing chromo-alumino-povondraite coming from the same locality as the present sample. Note that due to the relatively low concentrations of Fe, uncertainty on its oxidation state has little influence on the overall charge calculations. The (OH) content can then be calculated by charge balance with the assumption $T + Y + Z = 15.00$. The atomic proportions were calculated on this assumption (Table 6). The excellent match between the number of electrons per formula unit (epfu) derived from chemical and structural analysis supports this procedure, respectively: 251.2 and 251.3 epfu.

Table 6. Chemical composition of vanadio-oxy-dravite

	wt%		apfu
SiO_2	35.34(17)	Si	6.00(3)
TiO_2	0.29(4)	Ti^{4+}	0.037(5)
B_2O_3[a]	10.23	B	3.00
Al_2O_3	20.36(37)	Al	4.08(6)
Cr_2O_3	1.48(28)	Cr^{3+}	0.20(4)
V_2O_3	15.97(39)	V^{3+}	2.18(5)
Fe_2O_3[b]	0.34	Fe^{3+}	0.044(4)
FeO[b]	0.15	Fe^{2+}	0.021(3)
MgO	9.65(10)	Mg	2.44(3)
CaO	1.24(7)	Ca	0.23(1)
Na_2O	2.11(6)	Na	0.70(2)
K_2O	0.09(1)	K	0.019(2)
H_2O*	2.86	OH	3.26
Total	100.12		

Notes: Errors for oxides are standard deviations (in parentheses) of 10 spot analyses. Standard errors for the atomic proportions (in parentheses) were calculated by error-propagation theory; apfu = atoms per formula unit.
[a] Calculated by stoichiometry.
[b] Calculated as $Fe^{3+}/\Sigma Fe$ ratio = 0.68 (see text); measured FeO = 0.45(4).

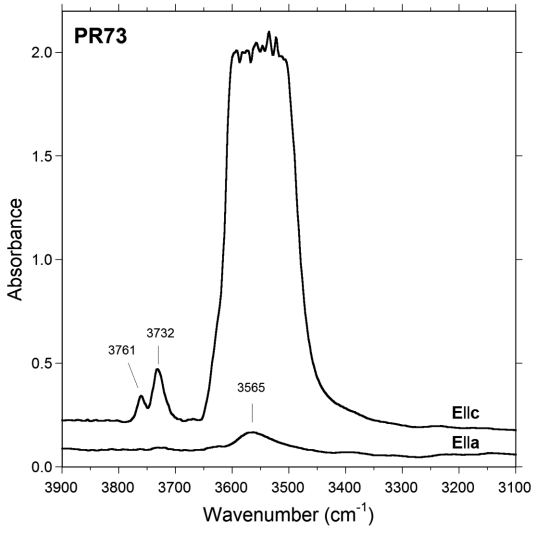

Figure 1. Polarized FTIR absorption spectra in the (OH)-stretching region of vanadio-oxy-dravite, vertically offset for clarity. Sample thickness 36 μm. The main band around 3550 cm^{-1} is truncated in the **c** direction due to excessive absorption.

Site populations

The anion site populations in the studied sample follow the general preference suggested for tourmaline (e.g., Grice and Ercit 1993; Henry et al. 2011): the O3 site (V position in the general formula) is occupied by (OH), and the O1 site (W position in the general formula) is occupied by O^{2-} and (OH). The cation distribution at the *T*, *Y*, and *Z* sites was optimized by using a quadratic program to minimize the residuals between calculated and observed data (based on the chemical and structural analysis). Site-scattering values, octahedral, and tetrahedral mean bond-distances (i.e., <*Y*-O>, <*Z*-O>, and <*T*-O>) were calculated as the linear contribution of each cation multiplied by its ideal bond-distance (Table 7). More details about the ideal distances as well as about the optimization procedure may be found in Bosi et al. (2004) and Bosi and Lucchesi (2004, 2007). The robustness of this approach was confirmed by another optimization procedure (Wright et al. 2000), which led to very similar cation distributions (Table 7). This result represents another example of convergence of these two procedures to similar solutions for tourmaline (e.g., Bosi and Lucchesi 2007; Filip et al. 2012; Bosi et al. 2012a, 2013a).

The final structural formulas are as follows:

$$^{X}(Na_{0.70}Ca_{0.23}\square_{0.05}K_{0.02})_{\Sigma 1.00}\ ^{Y}(V^{3+}_{1.39}Mg_{1.16}Al_{0.35}Fe^{3+}_{0.04}Ti^{4+}_{0.04}Fe^{2+}_{0.02})_{\Sigma 3.00}\ ^{Z}(Al_{3.74}Mg_{1.28}V^{3+}_{0.78}Cr^{3+}_{0.20})_{\Sigma 6.00}\ ^{T}(Si_{6.00}O_{18})\ ^{B}(BO_3)_3\ ^{V}(OH)_3\ ^{W}[O_{0.74}(OH)_{0.26}]_{\Sigma 1.00}.$$

The bond-valence analysis is consistent with the optimized structural formulas. Bond-valence calculations, using the formula and bond-valence parameters from Brown and Altermatt (1985), are reported in Table 8.

Name and crystal chemistry

The chemical composition of sample PR73 is consistent with tourmalines belonging to the alkali group, oxy-subgroup 3 (Henry et al. 2011). They are Na-dominant at the *X* site, oxygen-dominant at W with $O^{2-} > (OH+F)^{1-}$. As V^{3+} is the dominant cation at *Y* and Al^{3+} is the dominant cation at *Z*, its end-member composition may be represented as $NaV_3(Al_4Mg_2)Si_6O_{18}(BO_3)_3(OH)_3O$. This is in accord with the dominant-valency rule (Hatert and Burke 2008) for which the dominant ion of the dominant valency at one site becomes the basis for naming the species. As no tourmalines have yet been reported with V^{3+}- and Al^{3+}-dominant at *Y* and *Z*, respectively, this tourmaline can be classified as a new species. The closest end-member composition of a valid tourmaline species is that of oxy-dravite. The name vanadio-oxy-dravite may hence be

TABLE 7. Cation site populations (apfu), mean atomic numbers and mean bond lengths (Å) for vanadio-oxy-dravite

Site	Site population	Mean atomic number		Mean bond length	
		refined	calculated	refined	calculated[a]
X	0.70 Na + 0.23 Ca + 0.05 □ + 0.02 K	12.51(8)	12.52		
Y	1.39 V^{3+} + 1.16 Mg + 0.35 Al + 0.04 Fe^{3+} + 0.04 Ti^{4+} + 0.02 Fe^{2+}	17.64(7)	17.65	2.027	2.032
	(1.39 V^{3+} + 1.20 Mg + 0.30 Al + 0.04 Fe^{3+} + 0.04 Ti^{4+} + 0.02 Fe^{2+})[b]				
Z	3.73 Al + 1.28 Mg + 0.78 V^{3+} + 0.20 Cr^{3+}	14.48(4)	14.46	1.957	1.955
	(3.77 Al + 1.24 Mg + 0.79 V^{3+} + 0.20 Cr^{3+})[b]				
T	6.00 Si	14[c]	14.00	1.620	1.620
B	3 B	5[c]	5		

Notes: apfu = atoms per formula unit.
[a] Calculated using the ionic radii of Bosi and Lucchesi (2007).
[b] Site populations optimized by the procedure of Wright et al. (2000).
[c] Fixed in the final stages of refinement.

TABLE 8. Bond-valence calculations (valence unit) for vanadio-oxy-dravite

Site	*X*	*Y*	*Z*	*T*	*B*	Σ
O1		$0.51^{\times 3}\rightarrow$				1.51
O2	$0.17^{\times 3}\downarrow$	$0.42^{\times 2}\downarrow\rightarrow$			0.96	1.98
O3		0.34	$0.40^{\times 2}\rightarrow$			1.13
O4	$0.07^{\times 3}\downarrow$			$0.99^{\times 2}\rightarrow$		2.05
O5	$0.10^{\times 3}\downarrow$			$0.94^{\times 2}\rightarrow$		1.98
O6		$0.45^{\times 2}\downarrow$	0.49	1.04		1.99
O7			0.49	1.07		
			0.43			1.99
O8			0.48		$1.00^{\times 2}\downarrow$	2.00
			0.52			
Σ	1.02	2.59	2.81	4.04	2.96	
MFV	1.17	2.62	2.79	4.00	3.00	

Note: MFV = mean formal valence from site populations.

TABLE 9. Selected properties of oxy-dravite, vanadio-oxy-dravite, and oxy-vanadium-dravite

	Oxy-dravite	Vanadio-oxy-dravite	Oxy-vanadium-dravite
a (Å)	15.9273(2)	16.0273(3)	16.1908(4)
c (Å)	7.2001(1)	7.2833(1)	7.4143(2)
V (Å^3)	1581.81(4)	1620.24(5)	1683.21(7)
Space group	*R*3*m*	*R*3*m*	*R*3*m*
Optic sign	Uniaxial (–)	Uniaxial (–)	Uniaxial (–)
ω	1.650(5)	1.693(5)	1.786(5)
ε	1.620(5)	1.673(5)	1.729(4)
Color	Dark red	Green	Black
Pleochroism	O = orange E = pink	O = yellow green E = pale olive green	O = deep brownish green E = yellow green
Reference	(1)	(2)	(3 and 4)

Note: (1) Bosi and Skogby (2013); (2) this study; (3) Reznitskii et al. (2001); (4) Bosi et al. (2013a).

assigned for the chemical composition, following Henry et al. (2011). The prefix *vanadio* represents the substitution of 3V^{3+} for 3Al in the root composition of oxy-dravite. Comparative data for vanadio-oxy-dravite, oxy-dravite, and oxy-vanadium-dravite are given in Table 9.

Although there exists a significant degree of V^{3+}, Al, and Mg disorder over the *Y* and *Z* sites, the structural formula of sample PR73 indicates a clear preference of V^{3+} for the *Y* site and Al for the *Z* site, while Mg shows only a slight preference for the *Z* site. Chromium, on the other hand, seems completely ordered at the *Z* site. The O1 site is dominated by O^{2-} with a relatively minor concentration of (OH). The presence of only minor concentrations of (OH) at O1 (~0.26 apfu) are consistent with both the observation of weak absorption bands at 3761 and 3732 cm^{-1} in the infrared spectrum (Fig. 1), i.e., the area typically ascribed to the O1 site (see below), and the equation proposed by Bosi (2013) to estimate the (OH) contents in tourmaline: ^{W}(OH) = [2 – 1.01×BVS(O1) – 0.21 – F] = 0.27 apfu.

End-member formula

Although the amount of Mg at *Z* is larger than that at *Y* (1.28 and 1.16 apfu, respectively), the formula of vanadio-oxy-dravite may also be approximated as $Na^{Y}(V_2^{3+}Mg)^{Z}(Al_4MgV^{3+})(Si_6O_{18})(BO_3)_3(OH)_3O$. Such a formula could represent the structural formula for vanadio-oxy-dravite, but is not an end-member formula. In fact, this composition has multiple cations at more than one site (i.e., V^{3+} and Mg over *Y* and *Z*), and hence is inconsistent with the characteristics of an ordered end-member formula as defined by Hawthorne (2002b). The most ordered site allocation of V^{3+}, Al, and Mg consistent with the empirical formula and the end-member definition is $Na^{Y}(V_3)^{Z}(Al_4Mg_2)(Si_6O_{18})(BO_3)_3(OH)_3O$. Note that the difference between these two formulas is solely in V^{3+}-Mg order-disorder; no difference occurs in chemical composition.

Infrared spectroscopy

Spectra recorded in polarized mode perpendicular and parallel to the crystallographic **c** axis show an intense broad band around 3550 cm^{-1} and two weaker bands at 3732 and 3761 cm^{-1}, all strongly polarized in the **c** direction (Fig. 1). As it was not possible to thin the sample sufficiently to avoid off-scale absorption for the main band, any possible fine structure cannot be discerned. However, in line with previous studies (Bosi et al. 2012b, 2013b), the band can be related to the local arrangement ($^{Y}V^{3+}$ ^{Z}R ^{Z}R)-O3, i.e., to the occurrence of (OH) at the V position of the tourmaline general formula (O3 site in the structure). The two weaker bands at ca. 3732 and 3761 cm^{-1} are consistent with the minor concentrations of (OH) (ca. 0.3 apfu) assigned to the W position (O1 site in the structure), and may be related to the local arrangements ^{Y}(Mg Mg Mg) and ^{Y}(Mg Mg R) (cf. Gonzalez-Carreño et al. 1988; Bosi et al. 2012b, 2013b).

Optical-absorption spectroscopy

The optical spectra of vanadio-oxy-dravite show two broad absorption bands at ca. 432 and 609 nm, superimposed on an intense UV absorption edge (Fig. 2). These absorption bands are ascribed to spin-allowed *d-d* transitions in octahedrally coordinated V^{3+}, in accord with similar bands observed for vanadio-oxy-chromium-dravite (Bosi et al. 2012c, 2014) at ca. 440 and 610 nm. In addition to the dominant V^{3+}-bands, two broad but weak absorption bands at ca. 765 and 1100 nm are observed in the **E**||**a**-spectrum. They are in accord with previous studies on the optical spectra of tourmaline (e.g., Smith 1978; Taran et al.

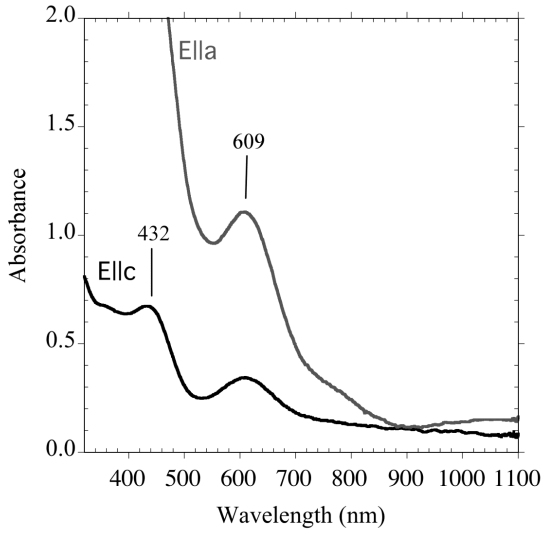

FIGURE 2. Polarized electronic absorption spectra for vanadio-oxy-dravite (sample PR73).

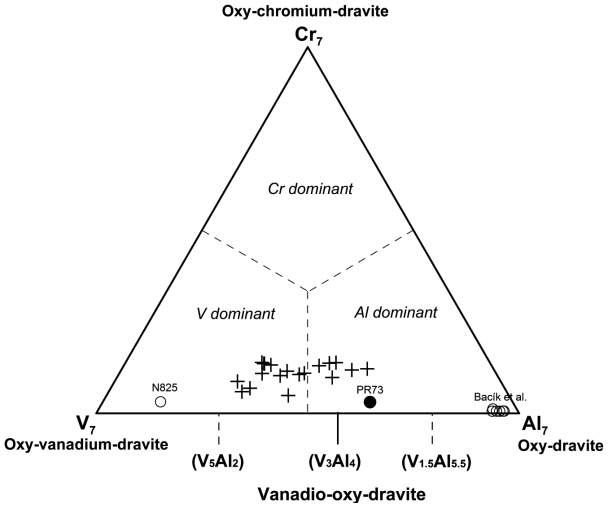

FIGURE 3. Ternary diagram in terms of Al-V-Cr at the $Y + Z$ sites for oxy-tourmalines. Black circle: present sample. Open circles: V^{3+}-bearing oxy-dravite samples with $V^{3+} > 0.20$ apfu (Bačík et al. 2011); and sample N825, oxy-vanadium-dravite (Bosi et al. 2013a); black crosses = vanadio-oxy-dravite samples from Sludyanka (Reznitsky et al. 2001).

1993; Mattson and Rossman 1987) and are ascribed to electronic transitions in Fe^{2+}-Fe^{3+} pairs. Consequently, the appearance of these absorption bands suggests that a small fraction of the total iron in the present sample occurs in the divalent state.

Compositional boundaries of vanadio-oxy-dravite

The plot of the *Z*- and *Y*-site cations in the ternary diagram for the Al-Cr-V^{3+} subsystem show, of course, that vanadio-oxy-dravite is ^{Z}Al-dominant and $^{Y}V^{3+}$-dominant. More interesting, however, is the triangular plot in terms of Al-Cr-V^{3+} at *Y* and *Z*, showing that vanadio-oxy-dravite can be either Al-dominant or V^{3+}-dominant (Fig. 3). This latter plot type displays the occurrence of three end-members along the full solid solution between the Al^{3+} and V^{3+} apices: oxy-dravite, vanadio-oxy-dravite, and oxy-vanadium-dravite. These end-members are related by the substitution $V^{3+} \leftrightarrow Al^{3+}$ at the Y position (vanadio-oxy-dravite $\leftrightarrow$ oxy-dravite) and $V^{3+} \leftrightarrow Al^{3+}$ at the Z position (oxy-vanadium-dravite $\leftrightarrow$ vanadio-oxy-dravite), while their compositional boundaries are at: (1) $^{Y+Z}(V_5Al_2)$, corresponding to $Na^{Y}(V_3)^{Z}(V_2Al_2Mg_2)Si_6O_{18}(BO_3)_3(OH)_3O$; (2) $^{Y+Z}(V_{1.5}Al_{5.5})$, corresponding to $Na^{Y}(V_{1.5}Al_{1.5})^{Z}(Al_4Mg_2)Si_6O_{18}(BO_3)_3(OH)_3O$. Consequently, oxy-dravite is characterized by V^{3+} contents less than 1.5 apfu, vanadio-oxy-dravite is characterized by V^{3+} contents between 5 and 1.5 apfu, and oxy-vanadium-dravite is characterized by V^{3+} contents larger than 5 apfu.

The discovery of the new mineral vanadio-oxy-dravite provides new information on the crystal chemistry of the tourmaline supergroup. The current chemical data supports complete exchange of V^{3+}, Cr^{3+}, and Al in species of the tourmaline supergroup (Reznitsky et al. 2001; Bosi et al. 2004, 2013a, 2013b), and it shows that vanadio-oxy-dravite can be either V^{3+}-dominant or Al-dominant.

ACKNOWLEDGMENTS

Chemical analyses were done with the kind assistance of M. Serracino to whom the authors express their gratitude. L. Reznitskii was supported by a grant from the Russian Foundation for Basic Research (project 13-05-00258). We thank the reviewers Darrel Henry and Frank C. Hawthorne for useful suggestions that improved the manuscript. The manuscript handling by Daniel Harlov is acknowledged.

REFERENCES CITED

Agrosì, G., Bosi, F., Lucchesi, S., Melchiorre, G., and Scandale, E. (2006) Mn-tourmaline crystals from island of Elba (Italy): Growth history and growth marks. American Mineralogist, 91, 944–952.

Bačík, P., Méres Š., and Uher, P. (2011) Vanadium-bearing tourmaline in metacherts from Chvojnica, Slovak Republic: crystal chemistry and multistage evolution. Canadian Mineralogist, 49, 195–206.

Bačík, P., Uher, P., Ertl, A., Jonsson, E., Nysten, P., Kanický, V., and Vaculovič, T. (2012) Zoned REE enriched dravite from a granitic pegmatite in Forshammar Bergslagen Province, Sweden an EMPA, XRD and LA-ICP-MS study. Canadian Mineralogist, 50, 825–841.

Bosi, F. (2008) Disordering of Fe^{2+} over octahedrally coordinated sites of tourmaline. American Mineralogist, 93, 1647–1653.

——— (2010) Octahedrally coordinated vacancies in tourmaline: a theoretical approach. Mineralogical Magazine, 74, 1037–1044.

——— (2011) Stereochemical constraints in tourmaline: from a short-range to a long-range structure. Canadian Mineralogist, 49, 17–27.

——— (2013) Bond-valence constraints around the O1 site of tourmaline. Mineralogical Magazine, 77, 343–351.

Bosi, F., and Lucchesi, S. (2004) Crystal chemistry of the schorl-dravite series. European Journal of Mineralogy, 16, 335–344.

——— (2007) Crystal chemical relationships in the tourmaline group: structural constraints on chemical variability. American Mineralogist, 92, 1054–1063.

Bosi, F., and Skogby, H. (2013) Oxy-dravite, $Na(Al_2Mg)(Al_5Mg)(Si_6O_{18})(BO_3)_3(OH)_3O$, a new mineral species of the tourmaline supergroup. American Mineralogist, 98, 1442–1448.

Bosi, F., Lucchesi, S., and Reznitskii, L. (2004) Crystal chemistry of the dravite-chromdravite series. European Journal of Mineralogy, 16, 345–352.

Bosi, F., Balić-Žunić, T., and Surour, A.A. (2010) Crystal structure analysis of four tourmalines from the Cleopatra's Mines (Egypt) and Jabal Zalm (Saudi Arabia), and the role of Al in the tourmaline group. American Mineralogist, 95, 510–518.

Bosi, F., Reznitskii, L., and Skogby, H. (2012a) Oxy-chromium-dravite, $NaCr_3(Cr_4Mg_2)(Si_6O_{18})(BO_3)_3(OH)_3O$, a new mineral species of the tourmaline supergroup. American Mineralogist, 97, 2024–2030.

Bosi, F., Skogby, H., Agrosì, G., and Scandale, E. (2012b) Tsilaisite, $NaMn_3Al_6(Si_6O_{18})(BO_3)_3(OH)_3OH$, a new mineral species of the tourmaline supergroup from Grotta d'Oggi, San Pietro in Campo, island of Elba, Italy. American Mineralogist, 97, 989–994.

Bosi, F., Reznitskii, L., Skogby, H., and Hålenius, U. (2012c) Vanadio-oxy-chromium-dravite IMA 2012-034. CNMNC Newsletter No. 14, October 2012, page 1286; Mineralogical Magazine, 76, 1281–1288.

Bosi, F., Reznitskii, L., and Sklyarov, E.V. (2013a) Oxy-vanadium-dravite,

$NaV_3(V_4Mg_2)(Si_6O_{18})(BO_3)_3(OH)_3O$: crystal structure and redefinition of the "vanadium-dravite" tourmaline. American Mineralogist, 98, 501–505.

Bosi, F., Skogby, H., Hålenius, U., and Reznitskii, L. (2013b) Crystallographic and spectroscopic characterization of Fe-bearing chromo-alumino-povondraite and its relations with oxy-chromium-dravite and oxy-dravite. American Mineralogist, 98, 1557–1564.

Bosi, F., Reznitskii, L., Skogby, H., and Hålenius, U. (2014) Vanadio-oxy-chromium-dravite, $NaV_3(Cr_4Mg_2)(Si_6O_{18})(BO_3)_3(OH)_3O$, a new mineral species of the tourmaline supergroup. American Mineralogist, 99, in press, DOI: 10.2138/am.2014.4568.

Brown, I.D., and Altermatt, D. (1985) Bond-valence parameters obtained from a systematic analysis of the Inorganic Crystal Structure Database. Acta Crystallographica, B41, 244–247.

Dutrow, B.L., and Henry, D.J. (2011) Tourmaline: A geologic DVD. Elements, 7, 301–306.

Filip, J., Bosi, F., Novák, M., Skogby, H., Tuček, J., Čuda, J., and Wildner, M. (2012) Redox processes of iron in the tourmaline structure: example of the high-temperature treatment of Fe^{3+}-rich schorl. Geochimica et Cosmochimica Acta, 86, 239–256.

Foit, F.F. Jr. (1989) Crystal chemistry of alkali-deficient schorl and tourmaline structural relationships. American Mineralogist, 74, 422–431.

Gonzalez-Carreño, T., Fernandez, M., and Sanz, J. (1988) Infrared and electron micropobe analysis in tourmalines. Physics and Chemistry of Minerals, 15, 452–460.

Grice, J.D., and Ercit, T.S. (1993) Ordering of Fe and Mg in the tourmaline crystal structure: the correct formula. Neues Jahrbuch für Mineralogie, Abhandlungen, 165, 245–266.

Hatert, F., and Burke, E.A.J. (2008) The IMA-CNMNC dominant-constituent rule revisited and extended. Canadian Mineralogist, 46, 717–728.

Hawthorne, F.C. (1996) Structural mechanisms for light-element variations in tourmaline. Canadian Mineralogist, 34, 123–132.

——— (2002a) Bond-valence constraints on the chemical composition of tourmaline. Canadian Mineralogist, 40, 789–797.

——— (2002b) The use of end-member charge-arrangements in defining new mineral species and heterovalent substitutions in complex minerals. Canadian Mineralogist, 40, 699–710.

Hawthorne, F.C., and Henry, D. (1999) Classification of the minerals of the tourmaline group. European Journal of Mineralogy, 11, 201–215.

Henry, D.J., and Dutrow, B.L. (2011) The incorporation of fluorine in tourmaline: Internal crystallographic controls or external environmental influences? Canadian Mineralogist, 49, 41–56.

Henry, D.J., Novák, M., Hawthorne, F.C., Ertl, A., Dutrow, B., Uher, P., and Pezzotta, F. (2011) Nomenclature of the tourmaline supergroup minerals. American Mineralogist, 96, 895–913.

Lussier, A.J., Aguiar, P.M., Michaelis, V.K., Kroeker, S., Herwig, S., Abdu, Y., and Hawthorne, F.C. (2008) Mushroom elbaite from the Kat Chay mine, Momeik, near Mogok, Myanmar: I. Crystal chemistry by SREF, EMPA, MAS NMR and Mössbauer spectroscopy. Mineralogical Magazine, 72, 747–761.

Lussier, A.J., Hawthorne, F.C., Aguiar, P.M., Michaelis, V.K., and Kroeker, S. (2011a) Elbaite-liddicoatite from Black Rapids glacier, Alaska. Periodico di Mineralogia, 80, 57–73.

Lussier, A.J., Abdu, Y. Hawthorne, F.C., Michaelis, V.K., Aguiar, P.M., and Kroeker, S. (2011b) Oscillatory zoned liddicoatite from Anjanabonoina, central Madagascar. I. Crystal chemistry and structure by SREF and ^{11}B and ^{27}Al MAS NMR spectroscopy. Canadian Mineralogist, 49, 63–88.

Mandarino, J.A. (1976) The Gladstone-Dale relationship. Part I: derivation of new constants. Canadian Mineralogist, 14, 498–502.

——— (1981) The Gladstone-Dale relationship. Part IV: the compatibility concept and its application. Canadian Mineralogist, 19, 441–450.

Mattson, S.M., and Rossman, G.R. (1987) Fe^{2+}-Fe^{3+} interactions in tourmaline. Physics and Chemistry of Minerals, 14, 163–171.

Novák, M., Povondra, P., and Selway, J.B. (2004) Schorl-oxy-schorl to dravite-oxy-dravite tourmaline from granitic pegmatites; examples from the Moldanubicum, Czech Republic. European Journal of Mineralogy, 16, 323–333.

Novák, M., Škoda, P., Filip, J., Macek, I., and Vaculovič, T. (2011) Compositional trends in tourmaline from intragranitic NYF pegmatites of the Tøebíč Pluton, Czech Republic; electron microprobe, Mössbauer and LA-ICP-MS study. Canadian Mineralogist, 49, 359–380.

Pouchou, J.L., and Pichoir, F. (1991) Quantitative analysis of homogeneous or stratified microvolumes applying the model "PAP." In K.F.J. Heinrich and D.E. Newbury, Eds., Electron Probe Quantitation, p. 31–75. Plenum, New York.

Reznitsky, L.Z., Sklyarov, E.V., Ushchapovskaya, Z.V., Nartova, N.V., Kashaev, A.A., Karmanov, N.S., Kanakin, S.V., Smolin, A.S., and Nekrosova, E.A. (2001) Vanadiumdravite, $NaMg_3V_6[Si_6O_{18}][BO_3]_3(OH)_4$, a new mineral of the tourmaline group. Zapiski Vsesoyuznogo Mineralogicheskogo Obshchestva, 130, 59–72 (in Russian).

Salnikova, E.B., Sergeev, S.A., Kotov, A.B., Yakovleva, S.Z., Steiger, R.H., Reznitskiy, L.Z., and Vasil'ev, E.P. (1998) U-Pb zircon dating of granulite metamorphism in the Slyudyanskiy complex, Eastern Siberia. Gondwana Research, 1, 195–205.

Sheldrick, G.M. (2008) A short history of SHELX. Acta Crystallographica, A64, 112–122.

Smith, G. (1978) A reassessment of the role of iron in the 5,000–30,000 cm^{-1} region of the electronic absorption spectra of tourmaline. Physics and Chemistry of Minerals, 3, 343–373.

Skogby, H., Bosi, F., and Lazor, P. (2012) Short-range order in tourmaline: a vibrational spectroscopic approach to elbaite. Physics and Chemistry of Minerals, 39, 811–816.

Taran, M.N., Lebedev, A.S., and Platonov, A.N. (1993) Optical absorption spectroscopy of synthetic tourmalines. Physics and Chemistry of Minerals, 20, 209–220.

van Hinsberg, V.J., and Schumacher, J.C. (2011) Tourmaline as a petrogenetic indicator mineral in the Haut-Allier metamorphic suite, Massif Central, France. Canadian Mineralogist, 49, 177–194.

van Hinsberg, V.J., Henry, D.J., and Marschall, H.R. (2011) Tourmaline: an ideal indicator of its host environment. Canadian Mineralogist, 49, 1–16.

Wright, S.E., Foley, J.A., and, Hughes, J.M. (2000) Optimization of site occupancies in minerals using quadratic programming. American Mineralogist, 85, 524–531.

Manuscript received May 17, 2013
Manuscript accepted August 19, 2013
Manuscript handled by Daniel Harlov